

ORIGINAL ARTICLE

Redoxtrons – An experimental system to study redox processes within the capillary fringe

Kristof Dorau¹  | Daniel Uteau²  | Markus Maisch³  |
 Andreas Kappler³  | Stephan Peth⁴  | Tim Mansfeldt¹ 

¹Department of Geosciences, Institute of Geography, University of Cologne, Köln, Germany

²Department of Soil Science, University of Kassel, Witzenhausen, Germany

³Department of Geosciences, University of Tuebingen, Tuebingen, Germany

⁴Institute of Soil Science, Leibniz University Hannover, Hannover, Germany

Correspondence

Kristof Dorau, Department of Geosciences, Institute of Geography, University of Cologne, Albertus-Magnus-Platz, D-50923 Köln, Germany.
 Email: k.dorau@uni-koeln.de

Daniel Uteau, Department of Soil Science, University of Kassel, Nordbahnhofstr. 1A, D-37213 Witzenhausen, Germany.
 Email: uteau@uni-kassel.de

Abstract

Spatiotemporal characterisation of the soil redox status within the capillary fringe (CF) is a challenging task. Air-filled porosities (ϵ), oxygen concentration (O_2) and soil redox potential (E_H) are interrelated soil variables within active biogeochemical domains such as the CF. We investigated the impact of water table (WT) rise and drainage in an undisturbed topsoil and subsoil sample taken from a Calcaric Gleysol for a period of 46 days. We merged 1D (E_H and matric potential) and 2D (O_2) systems to monitor at high spatiotemporal resolution redox dynamics within self-constructed redoxtron housings and complemented the data set by a 3D pore network characterization using X-ray microtomography (X-ray μ CT). Depletion of O_2 was faster in the organic matter- and clay-rich aggregated topsoil and the CF extended >10 cm above the artificial WT. The homogeneous and less-aggregated subsoil extended only 4 cm above the WT as indicated by ϵ - O_2 - E_H data during saturation. After drainage, 2D O_2 imaging revealed a fast aeration towards the lower depths of the topsoil, which agrees with the connected ϵ derived by X-ray μ CT (ϵ_{CT_conn}) of 14.9% of the total porosity. However, small-scaled anoxic domains with O_2 saturation <5% were apparent even after lowering the WT (down to 0.25 cm² in size) for 23 days. These domains remained a nucleus for reducing soil conditions ($E_H < -100$ mV), which made it challenging to characterise the soil redox status in the CF. In contrast, the subsoil aeration reached O_2 saturation after 8 days for the complete soil volume. Values of ϵ_{CT_conn} around zero in the subsoil highlighted that soil aeration was independent of this parameter suggesting that other variables such as microbial activity must be considered when predicting the soil redox status from ϵ alone. The use of redoxtrons in combination with localised redox-measurements and image based pore space analysis resulted in a better 2D/3D characterisation of the pore system and related O_2 transport properties. This allowed us to analyse the distribution and

Kristof Dorau and Daniel Uteau contributed equally to this work.

This is an open access article under the terms of the [Creative Commons Attribution-NonCommercial-NoDerivs](https://creativecommons.org/licenses/by-nc-nd/4.0/) License, which permits use and distribution in any medium, provided the original work is properly cited, the use is non-commercial and no modifications or adaptations are made.

© 2023 The Authors. *European Journal of Soil Science* published by John Wiley & Sons Ltd on behalf of British Society of Soil Science.

activity of microbiological niches highly associated with the spatiotemporal variable redox dynamics in soil environments.

Highlights:

- The time needed to turn from reducing to oxidising (period where all platinum electrodes feature $E_H > 300$ mV) condition differ for two samples with contrasting soil structure.
- The subsoil with presumably low O_2 consumption rates aerated considerably faster than the topsoil and exclusively by O_2 diffusion through medium- and fine-sized pores.
- To derive the soil redox status based upon the triplet ϵ - O_2 - E_H is challenging at present in heterogeneous soil domains and larger soil volumes than 250 cm^3 .
- Undisturbed soil sampling along with 2D/3D redox measurement systems (e.g., redoxtrons) improve our understanding of redox dynamics within the capillary fringe.

KEYWORDS

environmental monitoring, incubation experiments, redox processes, soil reducing conditions, undisturbed soil, X-ray microtomography

1 | INTRODUCTION

Capillary fringes (CF) are highly dynamic biogeochemical domains because fluctuating water tables continuously relocate the position between oxic and anoxic soil conditions. With focus on redox-related processes, triggered by oxygen (O_2) consumption and thereupon soil redox potential (E_H) decrease, the spatiotemporal extent of the CF has been rarely investigated at present. From a soil physical perspective, the CF is defined as the soil–air–water continuum and extends from the water table up to the limit of the capillary rise of water (Berkowitz et al., 2004). From a biogeochemical perspective, it is an oxic-anoxic interface where the O_2 distribution varies at the microscale due to the simultaneous O_2 supply from the atmosphere and the O_2 consumption via microbial and root respiration. Both processes can occur in close vicinity to each other and depend on the microscale soil structure. Thus, redox processes vary in space and time and an accurate representation demands (i) undisturbed soil samples with intact soil structure and (ii) at best 3D information on the pore system, derived, for example, by X-ray microtomography (X-ray μ CT) imaging (Dorau, Uteau, et al., 2021; Wanzek et al., 2018). Even though non-invasive imaging techniques have made significant progress in recent years to study dynamic 3D soil pore spaces (Peth, 2014), this scientific field needs to be developed towards studying pore space associated dynamic soil functions such as aeration-dependent redox processes.

A multitude of environmental parameters control the onset of reducing conditions within temporarily and permanently water-saturated soils and specifically in the CF. Hence, a detailed spatiotemporal characterisation of parameters that define the soil redox status is mandatory. The drivers to determine the E_H variability are manifold and comprise biotic and abiotic components, for instance, soil temperature (Hindersmann & Mansfeldt, 2014), thereupon microbial activity (Nikolausz et al., 2008), the availability of O_2 (Callebaut et al., 1982; Uteau et al., 2015), soil water content (θ) and related the air-filled pore space (ϵ) (Dorau et al., 2018; Dorau, Uteau, et al., 2021). Different sensor types must be combined to extend our knowledge of redox processes under in-situ conditions and obtain a cohesive assemblage of parameters stated above. Criteria for the choice of sensors include (i) its accuracy and precision for the measurement, (ii) from which volume of soil the information is derived, (iii) costs and (iv) the number of dimensions to consider. There is still debate at which level discrete single point measurements can adequately reflect natural in-situ conditions. As stated above, 3D investigation of structure related processes would be optimal but most of the sensors applied in soil science reflect discrete single point measurements, that is, a 1D needle type sensor. Examples for 1D sensors are platinum (Pt) tip electrodes. Quite recently, planar optodes gained attraction being able to acquire 2D images of the O_2 distribution up to the

μm range, which showed to improve our knowledge on rhizosphere related microbial processes (Koop-Jakobsen et al., 2018; Maisch et al., 2019) or O_2 transport within the CF (Haberer et al., 2015). Generally, we can expect an information gain from discrete single point measurements (e.g., by sensors placed within a specific depth), over area-based 2D imaging (e.g., to display a continuum by planar optodes), towards volume X-ray μCT 3D imaging (e.g., to account for pore architecture and soil heterogeneity).

This study builds upon two previous studies based on knowledge gain and complexity of the applied methods. Whereas the first study aimed at constructing a relationship between E_{H} and ε we encountered and highlighted the methodological shortcoming that it was not possible to resolve both parameters at the same location (Dorau et al., 2018). Thus, the second study employed X-ray μCT and image analysis to resolve the $E_{\text{H}}-\varepsilon$ relation via measurement of ε simultaneously to the soil aeration process and found that the connected air-filled porosity ($\varepsilon_{\text{CT,conn}}$) is a critical parameter for the aeration process (Dorau, Uteau, et al., 2021). Koestel et al. (2020) suggested that larger soil samples should be used to investigate dynamic processes that depend on the pore network connectivity – which certainly is true for the process of soil aeration. Thus, in this paper, we focus on soil aeration at a larger sample size to investigate how O_2 distribution accounts for redox dynamics within the CF at more representative sample volume. To do so we took undisturbed soil monoliths ($20 \times 20 \times 5$ cm) from the topsoil and the subsoil of a Calcaric Gleysol that differ in soil structure, mineral composition and soil organic matter (SOM) content. Self-constructed Plexiglas containers and a range of direct and indirect techniques, covering 1D to 3D measurements, enabled us to study the interaction of redox related processes within the CF. Following rhizosphere-related studies where *rhizotrons* (from Greek *rhízōma* = mass of roots) are used, our experimental incubation system is referred to as *redoxtron* in which the relationship between soil structure, O_2 distribution and E_{H} can be studied under controlled conditions. The redoxtrons were equipped with sensors to measure E_{H} , and matric potential (1D system), planar optodes to measure O_2 distribution (2D) and finally X-ray μCT and image analysis for a 3D pore network characterisation to obtain changes in air-filled porosity (ε_{CT}) and their connected fraction ($\varepsilon_{\text{CT,conn}}$).

2 | MATERIALS AND METHODS

2.1 | Excavation of soil monoliths

Soil sampling was conducted at Polder Speicherkoog in Northern Germany ($54^{\circ}8'1''\text{N}$; $8^{\circ}58'28''\text{E}$). The soil is a

Calcaric Gleysol (Eutric) according to WRB (IUSS Working Group WRB, 2015) and particularly suitable for the planned investigation because of frequent fluctuations of the near-surface groundwater table (Dorau & Mansfeldt, 2016; Dorau et al., 2018; Table 1). Thus, microorganisms are adapted to a temporary lack of O_2 . Redoxtrons were made of transparent Plexiglas (6 mm thickness; internal dimensions of $20 \times 20 \times 5$ cm; L/H/W) and brass screws were used to give the housing extra rigidity during the excavation of the soil monolith. A soil pit was excavated and the redoxtron housing without the front-panel pushed inside the topsoil (5–25 cm) and the subsoil (35–55 cm) until the soil got in contact with the back-panel (Figure 1a; see workflow in Figure S1; images in Figure S2). Afterwards, the soil-filled redoxtron was cut-off with a spade from the soil profile and transported to the laboratory within foam boxes to minimise a collapse of the pore network during transport. Prior to the start of the experiment, the soil surface facing towards the front panel of the Plexiglas was carefully prepared by a razor blade, scissor and spatula. Thereby, we aimed to minimise disturbance of the soil structure by clogging and smearing and obtain an even soil surface before the housing was sealed with the front-panel, which is especially important for installation of the planar optodes to measure O_2 (Figures S1 and S2; see Chapter 2.3). The samples were stored at 4°C until the experiment started to prevent mould, which was 1 month for the topsoil and 3 months for the subsoil. No water dripped out of the soil and, thus, the soil water content was below field capacity (see dotted line in Figure S7) prior to the start of the experiment.

2.2 | E_{H} and ε measurements (1D)

Soil redox potential measurements were performed by permanently installed Pt electrodes in duplicate and depths of 2.5, 7.5, 12.5 and 17.5 cm below soil surface. The Pt electrodes were embedded in a carbon fibre body (6-mm diameter) with a small-sized tip (5-mm length and 1-mm diameter; ecoTech, Bonn, Germany). We predrilled a small borehole that matches the diameter of the carbon fibre body down to 2, 7, 12 and 17 cm and pushed the tip gently into the undisturbed soil, respectively. The Pt electrodes were connected to a separated silver-silver chloride (Ag-AgCl) reference electrode (ecoTech, Bonn, Germany; 3 M KCl internal electrolyte). The E_{H} data were adjusted to the standard hydrogen electrode by adding 207 mV and we did not correct the E_{H} for any temperature dependency (Dorau, Bohn, et al., 2021), since soil temperature was constantly held at approximately 25°C . The Pt electrodes were tested for proper working prior and after the experiment without showing any deviation from the expected

TABLE 1 Soil description for the topsoil and subsoil sample.

	Sample	Topsoil	Subsoil
	Sampling depth (cm)	5 to 25 cm	35 to 55
Chemical properties	pH (–)	7.3 ± 0.1	7.4 ± 0.1
	Organic carbon content (g kg ⁻¹)	17.5 ± 0.92	4.6 ± 0.06
	Inorganic carbon content (g kg ⁻¹)	4.6 ± 0.31	5.9 ± 0.36
	Dithionite extractable iron (Fe _d ; g kg ⁻¹)	8.23 ± 0.22	1.92 ± 0.18
	Oxalate extractable iron (Fe _o ; g kg ⁻¹)	7.75 ± 0.19	0.88 ± 0.09
	Fe _o /Fe _d	0.94	0.46
	Oxalate extractable manganese (mg kg ⁻¹)	647 ± 24	16 ± 4
	S (mg kg ⁻¹)	640 ± 35	270 ± 23
Physical properties	Sand content (g kg ⁻¹)	130 ± 5	520 ± 3
	Silt content (g kg ⁻¹)	660 ± 8	360 ± 18
	Clay content (g kg ⁻¹)	210 ± 12	110 ± 9
	Textural class	Silt loam	Loamy sand
	Soil structure	Subangular blocky	Single grain
	Bulk density (g cm ⁻³)	1.16 ± 0.18	1.41 ± 0.13
Hydraulic properties	Water content at saturation (θ ₀ ; cm ³ cm ⁻³)	0.521 ± 0.005	0.446 ± 0.010
	Air-capacity (θ _{0-1.8} ; cm ³ cm ⁻³)	0.060 ± 0.003	0.025 ± 0.006
	Field-capacity (θ _{1.8-4.2} ; cm ³ cm ⁻³)	0.200 ± 0.036	0.280 ± 0.012
	Saturated hydraulic conductivity (cm day ⁻¹)	948 ± 112	50 ± 8

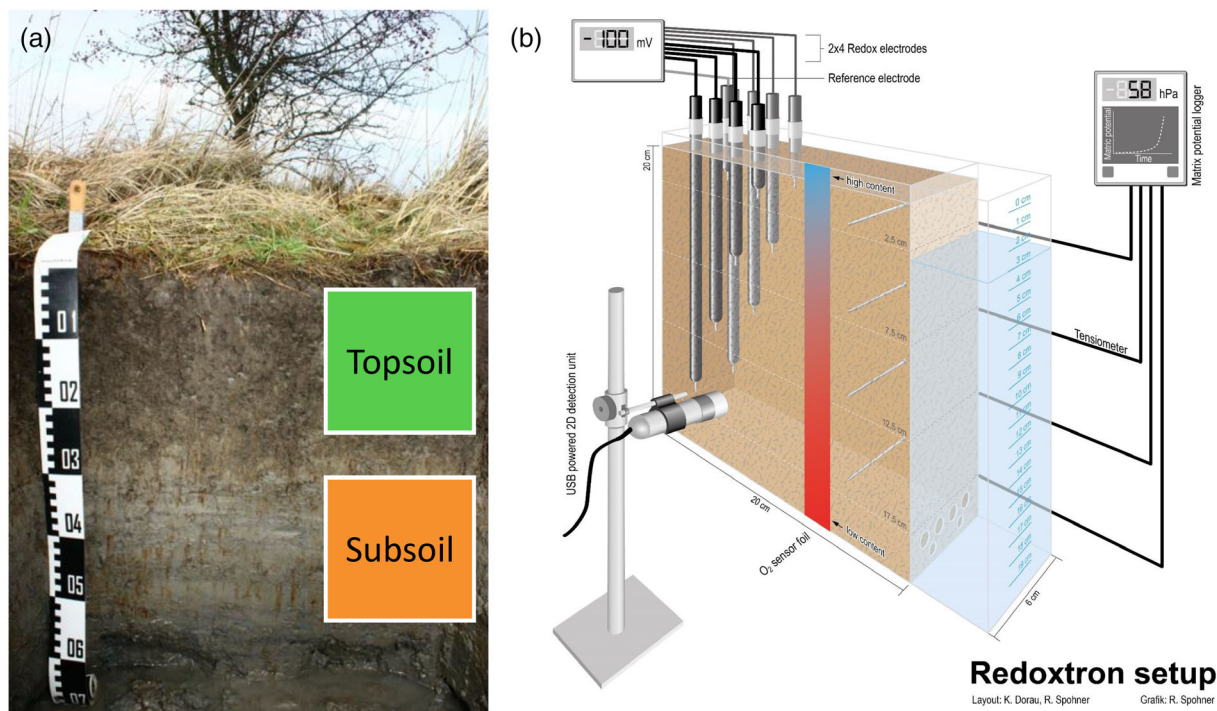


FIGURE 1 (a) Image of the Calcaric Gleysol (Eutric) from which an undisturbed topsoil (5 to 25 cm) and subsoil (35 to 55 cm) sample were obtained and (b) experimental redoxtron setup in which the undisturbed samples were incubated.

buffer solution value (± 5 mV; data not shown). Despite the long history of redox measurements in soils technical restrictions must be kept in mind and therefore, E_H measured by Pt electrodes are at best interpreted as “semi-quantitative expressions of mixed potentials in a non-equilibrium environment” (Austin & Huddleston, 1999; Mansfeldt, 2020). In case of our study, we are interested in the response of the measurement system to changes in O_2 due to water table rise and drainage of this system. Because the Pt electrode is very sensitive to aeration, this device is well-suited for our experimental design.

Soil matric potential (ψ_m) measurements by T5 microtensiometer (Meter, Munich, Germany) complemented the data. The ceramic tip was centred inside the soil sample from the back panel in the depths stated above. Based upon the available water retention curve from the topsoil and the subsoil (Figure S7), the Durner (1994) equation resulted in the lowest root mean square error for our retention data ($\theta_{RMSE} < 0.01$) and was used to calculate the volumetric water contents (θ ; $\text{cm}^3 \text{cm}^{-3}$):

$$\theta = w_1(1 + [a_1\psi_m]^{n_1})^{-m_1} + w_2(1 + [a_2\psi_m]^{n_2})^{-m_2} \quad (1)$$

where α , n and m are the van Genuchten parameters, ψ_m is the matric potential and w_1 and w_2 are weighting factors. Thereupon, we were able to calculate the air-filled porosity (ε ; $\text{cm}^3 \text{cm}^{-3}$) as:

$$\varepsilon = \theta_s - \theta \quad (2)$$

with θ_s being the volumetric water content at saturation ($\text{cm}^3 \text{cm}^{-3}$). The measurement interval was adjusted to 1 h throughout the incubation period.

2.3 | Planar optodes to measure O_2 (2D)

Non-invasive O_2 optodes were glued onto the inside of the front-panel with the fluorescing dye facing towards the soil (SF-RPSu4 and SF-HP5R, PreSens, Regensburg, Germany). The dimensions were 20 cm in height and 2.5 cm wide, enough to cover the height of the soil monolith. In front of the redoxtron, we positioned a camera detector (VisiSens TD, PreSens, Regensburg, Germany) in 30 cm distance and calibrated the sensor foils under ambient temperature in the laboratory ($\sim 25^\circ\text{C}$) within tap water. The redoxtron assembly with installed sensors and cabling was placed in a dark chamber to record under constant illumination without variations of daylight images of the 2D O_2 distribution. We took images in 1 h intervals because we expected a high dynamic in the system subsequent to water saturation.

2.4 | Experimental setup

All connections between the individual Plexiglas compounds were sealed with silicone gel to prevent leakage of water. A communication vessel besides the soil-filled housing enabled us to adjust the water table inside the redoxtron. The communication vessel featured an opening at the bottom (1 cm) to connect to the housing with the soil sample. We run the system for 1 week under oxidising soil conditions prior to rising the artificial water table with approximately 0.5 cm min^{-1} towards the centre of the soil monolith at 10 cm below surface (Figure 1b). From time to time we had to refill water until equilibrium was obtained with the water content inside the redoxtron and the communication vessel and secondly to compensate water loss due to evaporation. The experiment was run for 23 days with constant water table before we removed the water and re-aerated the soil. The lower boundary condition of the experiment was equivalent to seepage face, which simulates a groundwater table located at the bottom of the redoxtron during saturation and free gravity flow during drainage. Water was removed from the communication vessel with a syringe with approximately 0.5 cm min^{-1} , thus, at an equal rate similar to the artificial rise of the water table. Together with the aeration phase, the experiment lasted for 1.5 months and the topsoil and subsoil sample were measured sequentially.

2.5 | X-ray μCT image acquisition and analysis (3D)

We employed X-ray μCT to obtain a 3D model of the soil water distribution within the CF subsequent to the experiment by excavating a PVC liner (5 cm \varnothing and 20 cm height) from the redoxtron. X-ray μCT scans were done using a Zeiss Xradia 520 versa (Carl Zeiss Microscopy GmbH, Jena, Germany) at the Institute of Materials Science of the University of Hannover. Both liners were scanned at 160 keV energy and 7 W Power resulting in 1441 projections with an exposure time of 0.08 s in three-fold repetition. Three scans were vertically stitched to get the whole length of the sample with enough overlapping to prevent cone-beam artefacts. After reconstruction, the voxel edge length was $50 \mu\text{m}$. The borders and edges of the 3D-image were cut to contain finally 4.29 cm inner diameter of the liner. At both ends, we removed 20 slices thus having a final length of 19.8 cm. Image analysis was done using the software ImageJ and its plugin collection Fiji (Schindelin et al., 2012). For noise reduction, the non-local means denoising algorithm was used with default settings (Buades et al., 2011). This filter works

slice-wise (2D) like Gaussian blurring but preserves edges and boundaries. After filtering, the slices were stacked again in a 3D image. We used Otsu's algorithm (Otsu, 1979) to separate the soil matrix from resolved pores in a new binary image. The threshold was calculated slice-wise as there were grayscale gradients across the sample due to the cone-beam projections and the slice-wise filtering step. We accounted only for pores greater than 2 voxels in every direction to be sure having identified a real structure. To distinguish the X-ray μ CT resolved pores from the gravimetrically calculated porosity, we named it "CT-porosity". Furthermore, we quantified the fraction of the CT-porosity that was connected to the upper end of the sample, as O_2 would only be able to diffuse from the top of the sample when the drainage occurred (Section 2.4). To do that, we labelled every macropore with the "Connected Components Labelling" plugin of the MorphoLibJ package (Legland et al., 2016) and kept the largest one (by volume) so that all disconnected pores were removed. We called this "connected CT-porosity". The Local Thickness Plugin of ImageJ/Fiji was used to calculate the hydraulic equivalent diameter of the pores. The histogram of the resulting image was then the pore size distribution of the connected CT-porosity. By means of the measured matric potentials (Section 2.2) and applying the simplified Young-Laplace equation (diameter [μ m] = $3000 / \psi_m$ [hPa]) it was possible to calculate the actual air-filled CT-porosity (ϵ_{CT} , $\text{cm}^3 \text{cm}^{-3}$) and connected air-filled CT-porosity ($\epsilon_{CT, \text{conn}}$, $\text{cm}^3 \text{cm}^{-3}$). As we only were able to resolve pores larger than 100 μ m, we considered perfect aeration (no trapped air-bubbles). This was done for the monitored time points of interest subsequent to the drainage phase (each 0, 6, 12 h, 1, 2, 3, 4, 5 and 7 days for the topsoil and subsoil; Figure S3) and considering the four measured depths by segregating the soil columns into four parts (0–5, 5–10, 10–15 and 15–20 cm) yielding a vertical representation of the $\epsilon_{CT, \text{conn}}$. 3D renderings (Figure S6) were done with Paraview 5.7 (Kitware Inc., New York, USA).

2.6 | Chemical and physical soil properties

We took a representative and homogenised mixed sample (4 kg sample weight) within the open soil pit by a spatula from the top- (5–25 cm) and subsoil (35–55 cm) during the field campaign. The air-dried samples were sieved (< 2 mm \varnothing) and a part was milled to measure the following soil physicochemical properties: pH potentiometrically with a 0.01 M CaCl_2 solution mixed 5:1 with soil (v/v), the texture by the sieve and settling method, total carbon (TC), organic carbon (OC), inorganic carbon

(IC) and sulphur (S) by dry combustion with a CNS analyser (Vario EL cube, Elementar, Germany). Finally, $\text{Mn}^{\text{III,IV}}$ and Fe^{III} (oxyhydr)oxides were extracted by dithionite-citrate-bicarbonate (DCB) (Mehra & Jackson, 1960) and oxalate (Schwertmann, 1964). The extracts were measured by ICP-OES (SPECTROGREEN, Spectro, Kleve, Germany). Hydraulic properties were determined by undisturbed samples taken by 250 cm^3 steel cylinder (50 mm height and 80 mm \varnothing) within the centre of the topsoil (11 to 19 cm) and subsoil (41 to 49 cm), respectively. We used the evaporation method with a HYPROP device (Meter, Munich, Germany) to determine the water retention curve ($n = 3$) and a KSAT device (Meter, Munich, Germany) to measure the saturated hydraulic conductivity ($n = 8$). The bulk density was determined subsequently after drying of the soil within the steel cylinder at 105°C for 24 h and weighting afterwards.

3 | RESULTS

The soil temperature was nearly the same for both experiments with $21.7 \pm 0.68^\circ\text{C}$ for the topsoil and $22.9 \pm 0.70^\circ\text{C}$ for the subsoil (data not shown). As soon as we raised the water table within the redoxtrons to 10 cm depth, ϵ diminished in 17.5 and 12.5 cm but ranged between 0.011 and 0.050 $\text{cm}^3 \text{cm}^{-3}$ in 7.5 and 2.5 cm (Figure 2a and Figure S4). Whereas the O_2 concentration dropped to an average of $75 \pm 7.5\%$ in the 2.5 cm depth for the topsoil, no impact was observed for the subsoil with 100% O_2 saturation throughout the experiment (Figures 2b and 3). The redox data are coherent with the O_2 distribution since the E_H dropped among all depths subsequent to the decrease of O_2 (Figure S4 C to F). Thereby, strongly reducing conditions ($E_H < -100$ mV) were achieved in the 17.5 cm soil depth for both samples (Figure 2c and Figure S4 E to F) but the E_H did not drop in the 2.5 cm depth for the subsoil, in accordance with 100% O_2 saturation throughout the saturation phase.

After 23 days of drainage the topsoil featured anoxic conditions with < 5% O_2 saturation (Figure 3a) while ϵ was > 0.130 $\text{cm}^3 \text{cm}^{-3}$ throughout all depths (Figure S4A). Oxygen entered the soil from the surface in a gradual way following the decline of the water table (Figure 3b). The higher saturated hydraulic conductivity (> 900 cm d^{-1}) of the topsoil and a higher macropore fraction (Table 1) favoured the water drainage and subsequently the entering of O_2 down to 17.5 cm depth. During drainage, five of eight Pt electrodes characterised the soil milieu as oxidising ($E_H > 300$ mV) while three Pt electrodes did not detect O_2 in close vicinity of the Pt surface (Figure 4a) which shows the high heterogeneity of the examined topsoil. The

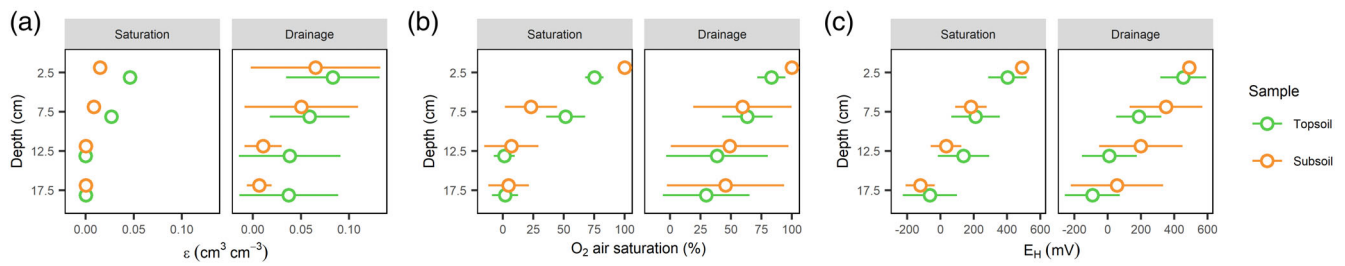


FIGURE 2 Air-filled porosity (ϵ ; a), oxygen saturation (O_2 ; b), and soil redox potential (E_H ; c) for the topsoil and subsoil redoxtron experiment. The data was aggregated for the saturation and drainage period with each 23 days of prevalence. Means and standard deviations are shown in each panel.

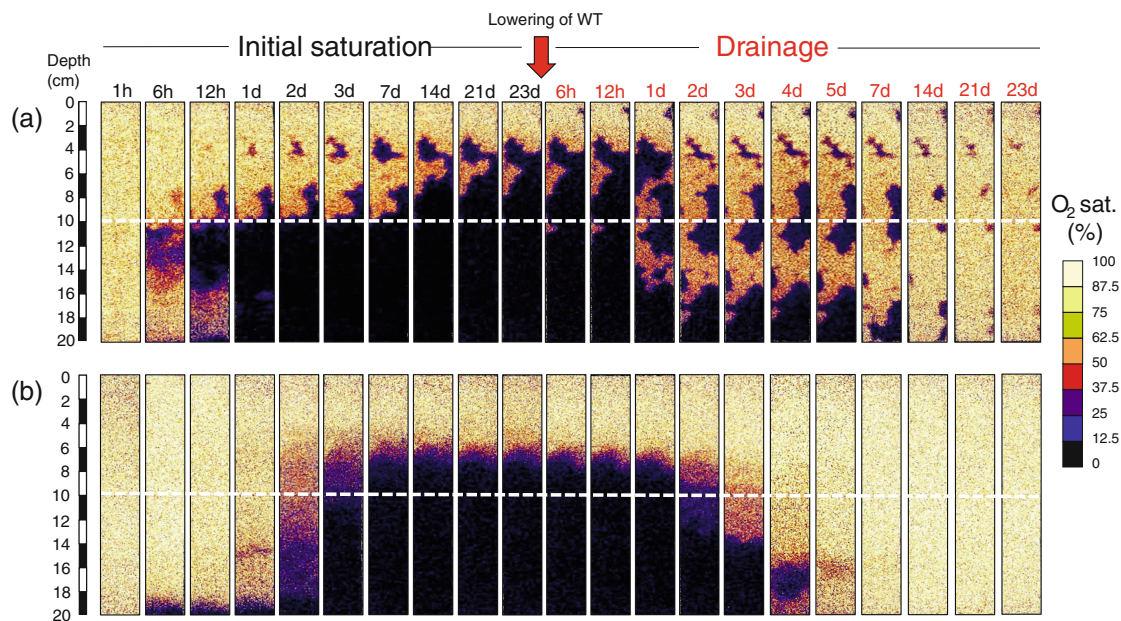


FIGURE 3 Images of the oxygen (O_2) distribution for a topsoil (a) and a subsoil (b) subsequently to water saturation (images featuring black numbers) and following to drainage (images featuring red numbers) at defined time scales. The red arrow marks the time point when the water was removed from the redoxtron, the colour gradient represents the O_2 concentration (saturation; in %), the scale marks 20 cm, and the white dotted line idealises the water table adjusted at 10 cm.

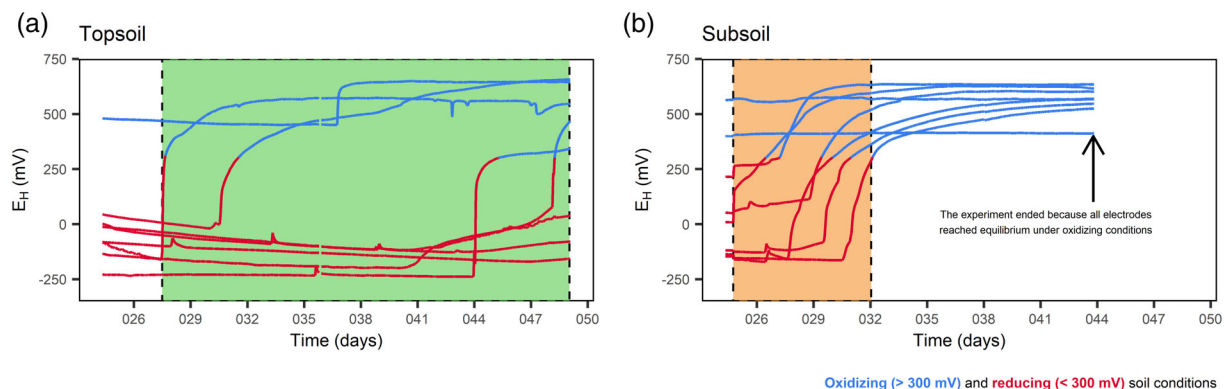


FIGURE 4 Soil redox potential (E_H) development for all Pt electrodes after drainage of water table in the redoxtron for the topsoil (a) and the subsoil (b). We defined the aeration phase from an initial response of a Pt electrode due to contact with O_2 until all Pt electrodes achieved oxidizing soil conditions with $E_H > 300$ mV. Please note, coloured boxes highlight the aeration phase subsequent to the WT decline (after 23 days). This period lasted only for 1 week for the subsoil and was not finished for the topsoil.

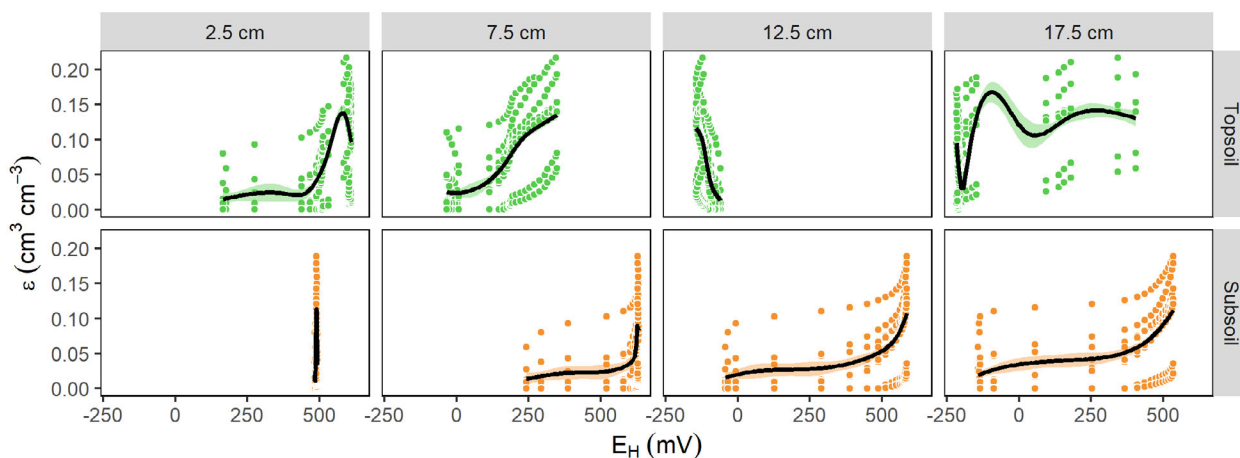


FIGURE 5 Air-filled porosity (ϵ) measured in the redoxtron plotted against soil redox potential (E_H) for the topsoil and subsoil sample among the depths in 2.5, 7.5, 12.5, and 17.5 cm. Black line is the loess regression smoothing to visualise the trend through the data.

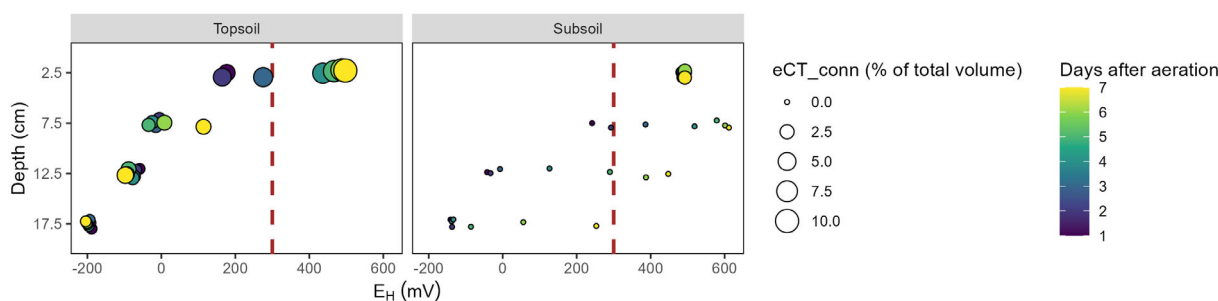


FIGURE 6 Spatiotemporal dynamics of ϵ_{CT_conn} and soil redox potential (E_H) for a topsoil and subsoil sample. Data accounts for the first 7 days of the aeration phase and the dashed brown line highlights the boundary between oxidising and reducing soil conditions.

subsoil turned from reducing to oxidising condition in 8 days (coloured box in Figure 4b) after which all Pt electrodes showed oxidising soil conditions (Figure 4b). The switch from reducing towards oxidising soil conditions was found in a narrow ϵ -window between 0.03 and 0.07 $\text{cm}^3 \text{cm}^{-3}$ of for the subsoil (Figure 5).

The soil near the surface, for both the topsoil and the subsoil, sample constituted the highest percentage of ϵ (Figure 7), which drastically decreased with soil depth below 2 cm and corresponds well to ϵ_{CT} and ϵ_{CT_conn} (Figures S5 and S6). On average for the complete soil core, ϵ_{CT} at field capacity (Figure S7, dotted line, where coarse pores are drained) was 15.5% with no significant differences compared with an ϵ_{CT_conn} of 14.9%. The subsoil featured a significantly smaller ϵ_{CT} of 3.33% and an ϵ_{CT_conn} of 1.3% (Figure 6). Whereas the topsoil featured a very well-connected air-filled pore system (ϵ_{CT_conn}) from the surface down to 20 cm depth, ϵ_{CT_conn} was absent below 3.5 cm for the subsoil (Figure 7 and Figure S5). Nevertheless, the related E_H showed that for the topsoil, only the upper part (0–5 cm depth) was under oxidising conditions 7 days after aeration, while for the

subsoil it was the case for almost the full sample (Figure 6).

4 | DISCUSSION

4.1 | Water table rise and impact on the CF

The redoxtron setup showed that during the saturation phase some air-filled pores remained for both the topsoil and subsoil within the CF. Within hours, microbial and root respiration started to consume the O_2 reservoir being present in the pore space and within 3 days subsequent to the water table rise strict anoxic conditions prevailed below the water table (Figure 3a,b). This confirms that soil depth (as a proxy for gas diffusion distances to the free atmosphere) and SOM content shifts the microbial community composition and activity and decreases the bacterial abundance with increasing soil depth (Hao et al., 2020), which would explain faster O_2 consumption rates in the topsoil with 4.8 times elevated SOM

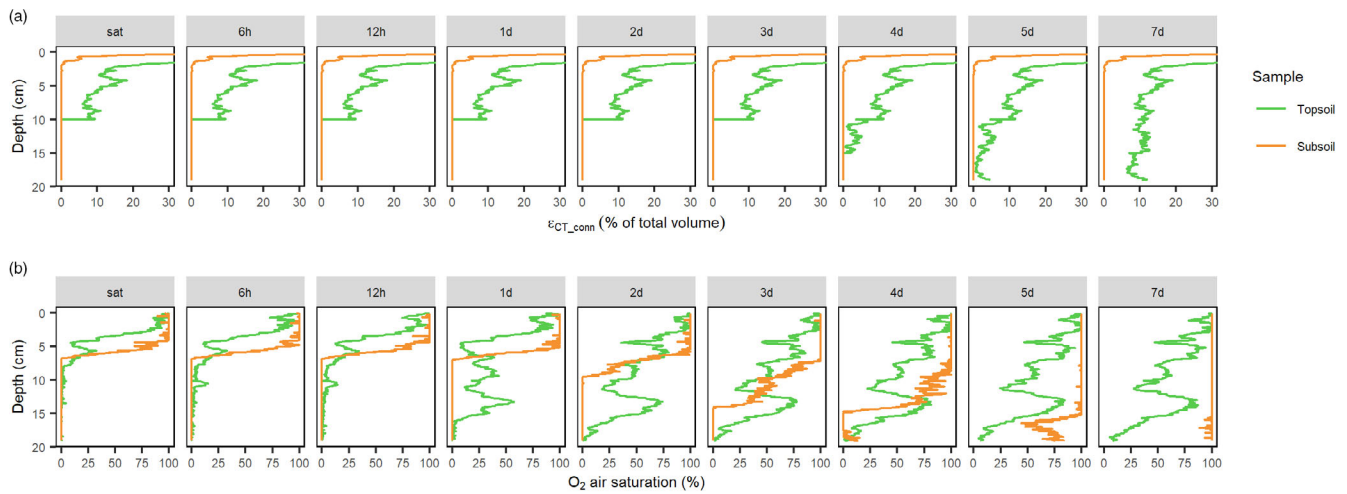


FIGURE 7 Spatiotemporal dynamics of ε_{CT_conn} and oxygen (O_2) distribution for a topsoil and subsoil sample starting from the water saturated state (left) to the first 7 days of the aeration phase.

compared to the subsoil (Figure 3 and Table 1). Both results of E_H and O_2 distribution suggest that the CF extends only 4 cm above the water table for the subsoil, while anoxic domains exist up to the soil surface for the topsoil (Figure 3a,b and Figure S4E). To delineate the extent of the CF by soil physical constrained parameters is difficult, since (i) the CF strongly depends on the retention characteristics altered by fractures and macropores, (ii) caution must be invoked in applying the concept to a fluctuating water table because of a lack in hydrostatic equilibrium and (iii) soil-water hysteresis would result in a different CF with rising water table compared with a falling water table (Nimmo, 2005). However, when including the soil redox status this becomes even more challenging due to two reasons: First, the spatial resolution of aeration sensors must be kept in mind, for example, the Pt electrode is small but the axis was long enough to reflect different aeration zones through inter- and intra-aggregate domains (Flühler et al., 1976; Zausig et al., 1993). Another intrinsic soil property is the clay content, which enhances the likelihood to detect anoxic microhabitats in a presumably oxidising soil environment, as higher structural heterogeneity (with the presence of well-connected inter-aggregate macropores and disconnected intra-aggregate meso/micropores) can be assumed (Keiluweit et al., 2018).

4.2 | Anoxic microsites dominate the drainage phase

Anoxic microsites in otherwise well-aerated soils were found to be negatively correlated to clay content, an effect attributed when O_2 consumption outpaces O_2

supply through diffusion (Keiluweit et al., 2018). Even though these small anoxic domains represented only a small proportion of the topsoil, they differed plausibly with the subsoil. This can be explained by lower clay and SOM contents of the subsoil (Table 1) that favoured a fast drainage together with a presumably lower microbial activity leading to enhanced O_2 diffusion from the top.

The E_H - ε relation is difficult to predict in the topsoil due to the clay-rich microstructure (Dorau, Uteau, et al., 2021) that characterised the sample – a feature to which Pt electrodes are particularly sensitive. Overall, characterisation of the aeration status in the CF might be misleading if only one parameter is considered from the ε - O_2 - E_H triplet. Structural properties of the gaseous diffusion paths as well as the spatiotemporal distribution of gaseous sinks and sources render an interpretation particularly complicated (Flühler et al., 1976). However, application of pedotransfer functions (PTFs) seem applicable for the E_H - ε relation in less aggregated soils, as our subsoil sample, allowing to predict the switch from reducing towards oxidising soil conditions. In addition, prediction of the soil redox status based upon ε might work for small sample volumes ($< 250 \text{ cm}^3$) in soils with structural pores (Dorau et al., 2018), but to tackle the dynamic processes taking place in a fluctuating CF seems far-fetched at present for larger samples ($> 2000 \text{ cm}^3$) of well-structured soils, as our topsoil (Figure 5).

4.3 | Pore network characteristics

Our main findings on the 3D pore network, namely that there is a higher extent of connective macroporosity in the topsoil compared to the subsoil, are counterintuitive to the

long time needed to switch from reducing to oxidising condition at the topsoil and a very narrow timespan at the subsoil (Figure 7). We assume that independent of the well-connected pore system that initialises a fast transport of O_2 towards the 17.5 cm depth after 2 days of drainage, anoxic microsites prevail up to 23 days and these remain a nucleus for reducing conditions. On the contrary, disconnected pores (in terms of the resolved pores by X-ray CT) in the subsoil do not necessarily prevent a fast soil aeration process as shown by the E_H readings (Figure 4b). This indicates that oxygenation and an increase in E_H from reducing towards oxidising conditions is a combined result of the microbial activity and aeration through macropores (and presumable pores that were not resolved by the achieved X-ray μ CT resolution that would drain at higher matric potentials).

4.4 | Undisturbed soil samples – A key to better understand dynamic redox processes

Recent attempts to characterise the CF more into detail with focus on redox dynamics and biogeochemical processes (e.g., nitrogen transformation) are very useful (Fiola et al., 2020). However, research in this respect should focus on undisturbed soil samples rather than using homogenised soil within repacked soil columns as commonly done (Farnsworth et al., 2012; Fiola et al., 2020; Rezanezhad et al., 2014; Tokunaga et al., 2018). This is important not only with respect to soil structure that changes significantly by homogenisation generating an artificial pore space but also to the accessibility and distribution of organic matter that plays a major role in redox dynamics. Obviously, a natural soil with a given soil architecture accounts for structural units featuring intra- and inter-aggregate domains, which can result in steep E_H and O_2 gradients (Keiluweit et al., 2018; Sexstone et al., 1985). Thereupon, roots alter the extent to which O_2 and E_H are influenced driven by the soil water content (Uteau et al., 2015). Undisturbed soil sampling maintains the soil architecture as it constraints physical, chemical and biological processes more realistic and is more of societal concern to understand soil functions (Vogel et al., 2022). Likewise, we know that organic matter is rather heterogeneously distributed in naturally structured soils (Peth et al., 2014) and this needs to be considered when drawing conclusions on the spatial heterogeneity of E_H and O_2 availability. Future efforts should be made to account for anoxic microsites in soil redox processes by (i) better mimicking field conditions using well-controlled experimental designs, (ii) including non-invasive imaging techniques and (iii) enhancing models accounting for the small scale spatial relationships between pores, organic matter and

microbial activity (Ngom et al., 2011; Zhang & Furman, 2021). In this study, we aimed to incorporate this behaviour while merging 1D, 2D and – at best – 3D operating systems to highlight spatiotemporal diverse redox dynamics taking place within the CF. Redoxtrons and the presented methodological approach can greatly contribute to better understanding the complex interplay between water table rise and drainage in temporarily water saturated soil environments. Our setup allows a more discrete characterisation of the spatiotemporal extent in the CF, which has the benefit to e.g., optimise sampling protocols for soil solution to investigate redox sensitive species and their relationship to environmental parameters investigated within this study. For instance, dynamics for the mobilisation or retention of redox sensitive trace metals (Fe^{2+}/Fe^{3+} and As^{3+}/As^{5+}) or improve models of trace gas evolution (N_2O/N_2 and CH_4/CO_2) based on observations that can complement our setup.

5 | CONCLUSIONS

Classically, field experiments that focus on redox dynamics utilise single point measurements (1D), while incubation experiments in the laboratory employ homogenised and repacked soil columns. Both factors neglect the complex interplay of dynamic variables, such as the triplet of air-filled pores, O_2 saturation and redox potential in temporarily water saturated soil environments. Redoxtrons feature a novel system with direct and indirect techniques covering 1D to 3D measurements that is capable to capture transient redox processes. A better understanding from the millimetre (e.g., aggregates) up to the decimetre (e.g., pedon) scale can be achieved – both in space and time. At the same time, this system avoids a misinterpretation of the soil redox status due to the small-scaled Pt electrode reading that has a high sensitivity to spatial heterogeneity. Using the redoxtron, we could relate physically constrained parameters that define the CF with information about the onset of reducing conditions, e.g., horizon-specific redox hysteresis as observed by non-uniformly behaviour during the saturation and the drainage phase. In this context, future studies might incorporate biogeochemical processes featuring the depth-dependent production of greenhouse gases, soil solution composition featuring redox-active metals, and fate of organic and inorganic contaminants and nutrients.

AUTHOR CONTRIBUTIONS

Kristof Dorau: Conceptualization; investigation; writing – original draft; methodology; formal analysis; data curation; visualization. **Daniel Uteau:** Investigation;

writing – original draft; methodology; formal analysis; visualization. **Markus Maisch:** Methodology; writing – review and editing. **Andreas Kappler:** Methodology; writing – review and editing; resources. **Stephan Peth:** Methodology; writing – review and editing. **Tim Mansfeldt:** Methodology; writing – review and editing; conceptualization; funding acquisition; supervision; resources.

ACKNOWLEDGEMENTS

We greatly acknowledge the support by Mr. Steffen Richter and Mr. Christian Dressel for support during construction of the redoxtron bodies, Dr. Regine Spohner for visualising the technical drawing of the experimental setup, Mrs. Karin Greef, Mrs. Maren Hövels, Mr. Constantin Lux, and Dr. Felix Brück were a great help during maintenance of the incubation experiment, and Dr. Robert Meier for support to analyse the O₂ data. Open Access funding enabled and organized by Projekt DEAL.

CONFLICT OF INTEREST STATEMENT

The authors declare that there is no conflict of interest that could be perceived as prejudicing the impartiality of the research reported.

DATA AVAILABILITY STATEMENT


The data that support the findings of this study are available from the corresponding author upon reasonable request.

ORCID

Kristof Dorau  <https://orcid.org/0000-0002-1815-1929>

Daniel Uteau  <https://orcid.org/0000-0003-1499-4344>

Markus Maisch  <https://orcid.org/0000-0002-4275-4957>

Andreas Kappler  <https://orcid.org/0000-0002-3558-9500>

Stephan Peth  <https://orcid.org/0000-0001-9799-212X>

Tim Mansfeldt  <https://orcid.org/0000-0002-7557-6827>

REFERENCES

- Austin, W. E., & Huddleston, J. H. (1999). Viability of permanently installed platinum redox electrodes. *Soil Science Society of America Journal*, 63, 1757–1762.
- Berkowitz, B., Silliman, S. E., & Dunn, A. M. (2004). Impact of the capillary fringe on local flow, chemical migration, and microbiology. *Vadose Zone Journal*, 3, 534–548.
- Buades, A., Bartomeu, C., & Morel, J. M. (2011). Non-local means Denoising. *Image Processing on Line*, 1, 208–212.
- Callebaut, F., Gabriels, D., Minjauw, W., & Boodt, M. D. (1982). Redox potential, oxygen diffusion rate, and soil gas composition in relation to water table level in two soils. *Soil Science*, 134, 149–156.
- Dorau, K., Bohn, B., Weihermüller, L., & Mansfeldt, T. (2021). Temperature-induced diurnal redox potential in soil. *Environmental Science: Processes & Impacts*, 23, 1782–1790.

- Dorau, K., Luster, J., & Mansfeldt, T. (2018). Soil aeration: The relation between air-filled pore volume and redox potential. *European Journal of Soil Science*, 69, 1035–1043.
- Dorau, K., & Mansfeldt, T. (2016). Comparison of redox potential dynamics in a diked marsh soil: 1990 to 1993 versus 2011 to 2014. *Journal of Plant Nutrition and Soil Science*, 179, 641–651.
- Dorau, K., Uteau, D., Hövels, M. P., Peth, S., & Mansfeldt, T. (2021). Soil aeration and redox potential as function of pore connectivity unravelled by X-ray microtomography imaging. *European Journal of Soil Science*, 73, 1–10.
- Durner, W. (1994). Hydraulic conductivity estimation for soils with heterogeneous pore structure. *Water Resources Research*, 30, 211–223.
- Farnsworth, C. E., Voegelin, A., & Hering, J. G. (2012). Manganese oxidation induced by water table fluctuations in a sand column. *Environmental Science & Technology*, 46, 277–284.
- Fiola, J. C., Rabenhorst, M. C., Scaduto, E., Seitz, C. R., & Rankin, K. M. S. (2020). Soil biogeochemistry of the capillary fringe in laboratory mesocosms with contrasting soil textures. *Soil Science Society of America Journal*, 84, 1011–1021.
- Flühler, H., Stolzy, L. H., & Ardakani, M. S. (1976). A statistical approach to define soil aeration in respect to denitrification. *Soil Science*, 122, 115–123.
- Haberer, C. M., Rolle, M., Cirpka, O. A., & Grathwohl, P. (2015). Impact of heterogeneity on oxygen transfer in a fluctuating capillary fringe. *Groundwater*, 53, 57–70.
- Hao, J., Chai, Y. N., Lopes, L. D., Ordóñez, R. A., Wright, E. E., Archontoulis, S., & Schachtman, D. P. (2020). The effects of soil depth on the structure of microbial communities in agricultural soils in Iowa, USA. *Applied and Environmental Microbiology*, 87, e02673–e02620.
- Hindersmann, I., & Mansfeldt, T. (2014). Trace element solubility in a multimetal-contaminated soil as affected by redox conditions. *Water, Air, & Soil Pollution*, 225, 1–20.
- Keiluweit, M., Gee, K., Denney, A., & Fendorf, S. (2018). Anoxic microsites in upland soils dominantly controlled by clay content. *Soil Biology and Biochemistry*, 118, 42–50.
- Koestel, J., Larsbo, M., & Jarvis, N. (2020). Scale and REV analyses for porosity and pore connectivity measures in undisturbed soil. *Geoderma*, 366, 114206.
- Koop-Jakobsen, K., Mueller, P., Meier, R. J., Liebsch, G., & Jensen, K. (2018). Plant-sediment interactions in salt marshes – An optode imaging study of O₂, pH, and CO₂ gradients in the rhizosphere. *Frontiers in Plant Science*, 9, 541.
- Legland, D., Arganda-Carreras, I., & Andrey, P. (2016). MorphoLibJ: Integrated library and plugins for mathematical morphology with ImageJ. *Bioinformatics*, 32, 3532–3534.
- Maisch, M., Lueder, U., Kappler, A., & Schmidt, C. (2019). Iron lung: How rice roots induce iron redox changes in the rhizosphere and create niches for microaerophilic Fe(II)-oxidizing bacteria. *Environmental Science & Technology Letters*, 6, 600–605.
- Mansfeldt, T. (2020). Soil redox potential. In S. Wessel-Bothe & L. Weihermüller (Eds.), *Field measurement methods in soil science* (pp. 19–41). Borntraeger Science Publishers.
- Mehra, O. P., & Jackson, M. L. (1960). Iron oxide removal from soils and clays by a dithionite-citrate system buffered with sodium bicarbonate. *Clays and Clay Minerals*, 7, 317–327.
- Ngom, N. F., Garnier, P., Monga, O., & Peth, S. (2011). Extraction of three-dimensional soil pore space from microtomography images using a geometrical approach. *Geoderma*, 163, 127–134.

- Nikolausz, M., Kappelmeyer, U., Székely, A., Ruzsnyák, A., Márialigeti, K., & Kästner, M. (2008). Diurnal redox fluctuation and microbial activity in the rhizosphere of wetland plants. *European Journal of Soil Biology*, *44*, 324–333.
- Nimmo, J. R. (2005). Unsaturated zone flow processes. In M. G. Anderson & J. McDonnell (Eds.), *Encyclopedia of hydrological sciences*. John Wiley & Sons Ltd.
- Otsu, N. (1979). A threshold selection method from gray-level histograms. *IEEE Transactions on Systems, Man, and Cybernetics*, *9*, 62–66.
- Peth, S. (2014). Noninvasive quantification of 3D pore space structures in soils. In J. Gliński, J. Horabik, & J. Lipiec (Eds.), *Encyclopedia of agrophysics* (pp. 516–520). Springer.
- Peth, S., Chenu, C., Leblond, N., Mordhorst, A., Garnier, P., Nunan, N., Pot, V., Ogurreck, M., & Beckmann, F. (2014). Localization of soil organic matter in soil aggregates using synchrotron-based X-ray microtomography. *Soil Biology and Biochemistry*, *78*, 189–194.
- Rezanezhad, F., Couture, R. M., Kovac, R., O'Connell, D., & Van Cappellen, P. (2014). Water table fluctuations and soil biogeochemistry: An experimental approach using an automated soil column system. *Journal of Hydrology*, *509*, 245–256.
- Schindelin, J., Arganda-Carreras, I., Frise, E., Kaynig, V., Longair, M., Pietzsch, T., Preibisch, S., Rueden, C., Saalfeld, S., Schmid, B., Tinevez, J.-Y., White, D. J., Hartenstein, V., Eliceiri, K., Tomancak, P., & Cardona, A. (2012). Fiji: An open-source platform for biological-image analysis. *Nature Methods*, *9*, 676–682.
- Schwertmann, U. (1964). Differenzierung der Eisenoxide des Bodens durch Extraktion mit Ammoniumoxalat-Lösung. *Zeitschrift für Pflanzenernährung, Düngung, Bodenkunde*, *105*, 194–202.
- Sexstone, A. J., Revsbech, N. P., Parkin, T. B., & Tiedje, J. M. (1985). Direct measurement of oxygen profiles and denitrification rates in soil aggregates. *Soil Science Society of America Journal*, *49*, 645–651.
- Tokunaga, T. K., Kim, Y., Wan, J., Bill, M., Conrad, M., & Dong, W. (2018). Method for controlling temperature profiles and water table depths in laboratory sediment columns. *Vadose Zone Journal*, *17*, 180085.
- Uteau, D., Hafner, S., Pagenkemper, S. K., Peth, S., Wiesenberg, G. L. B., Kuzyakov, Y., & Horn, R. (2015). Oxygen and redox potential gradients in the rhizosphere of alfalfa grown on a loamy soil. *Journal of Plant Nutrition and Soil Science*, *178*, 278–287.
- Vogel, H.-J., Balseiro-Romero, M., Kravchenko, A., Otten, W., Pot, V., Schlüter, S., Weller, U., & Baveye, P. C. (2022). A holistic perspective on soil architecture is needed as a key to soil functions. *European Journal of Soil Science*, *73*, e13152.
- Wanzek, T., Keiluweit, M., Varga, T., Lindsley, A., Nico, P., Fendorf, S., & Kleber, M. (2018). The ability of soil pore network metrics to predict redox dynamics is scale dependent. *Soil Systems*, *2*, 1–25.
- Zausig, J., Stepniewski, W., & Horn, R. (1993). Oxygen concentration and redox potential gradients in unsaturated model soil aggregates. *Soil Science Society of America Journal*, *57*, 908–916.
- Zhang, Z., & Furman, A. (2021). Redox dynamics at a dynamic capillary fringe for nitrogen cycling in a sandy column. *Journal of Hydrology*, *603*, 126899.

SUPPORTING INFORMATION

Additional supporting information can be found online in the Supporting Information section at the end of this article.

How to cite this article: Dorau, K., Uteau, D., Maisch, M., Kappler, A., Peth, S., & Mansfeldt, T. (2023). *Redoxtrons – An experimental system to study redox processes within the capillary fringe*. *European Journal of Soil Science*, *74*(1), e13347. <https://doi.org/10.1111/ejss.13347>